

On the role of the $\Gamma - \lambda_{\text{Edd}}$ relation on the X-ray Baldwin effect in Active Galactic Nuclei

C. Ricci^{1,2*}, S. Paltani¹, Y. Ueda² and H. Awaki³

¹Department of Astronomy, University of Geneva, ch. d'Ecogia 16, 1290 Versoix, Switzerland

²Department of Astronomy, Kyoto University, Oiwake-cho, Sakyo-ku, Kyoto 606-8502

³Department of Physics, Ehime University, Matsuyama, 790-8577, Japan

Received; accepted

ABSTRACT

The X-ray Baldwin effect is the inverse correlation between the equivalent width (EW) of the narrow component of the iron $K\alpha$ line and the X-ray luminosity of active galactic nuclei (AGN). A similar trend has also been observed between Fe $K\alpha$ EW and the Eddington ratio (λ_{Edd}). Using *Chandra*/HEG results of Shu et al. (2010) and bolometric corrections we study the relation between EW and λ_{Edd} , and find that $\log EW = (-0.13 \pm 0.03) \log \lambda_{\text{Edd}} + 1.47$. We explore the role of the known positive correlation between the photon index of the primary X-ray continuum Γ and λ_{Edd} on the X-ray Baldwin effect. We simulate the iron $K\alpha$ line emitted by populations of unabsorbed AGN considering 3 different geometries of the reflecting material: toroidal, spherical-toroidal and slab. We find that the $\Gamma - \lambda_{\text{Edd}}$ correlation cannot account for the whole X-ray Baldwin effect, unless a strong dependence of Γ on λ_{Edd} , such as the one recently found by Risaliti et al. (2009) and Jin et al. (2012), is assumed. No clear correlation is found between EW and Γ . We conclude that a good understanding of the slope of the $\Gamma - \lambda_{\text{Edd}}$ relation is critical to assess whether the trend plays a leading or rather a marginal role in the X-ray Baldwin effect.

Key words: Galaxies: Seyferts – X-rays: galaxies – Galaxies: active – Galaxies: nuclei

1 INTRODUCTION

The first evidence of the existence of a relation between the luminosity and the equivalent width (EW) of a line in active galactic nuclei (AGN) was found by Baldwin (1977) for the broad C IV $\lambda 1549$ emission line. This trend is usually called the *Baldwin effect*, and it has been found for several other optical, UV and IR lines (see Shields 2007 for a review). A possible explanation for the Baldwin effect of the lines produced in the broad line region (BLR) is that it is related to a luminosity-dependent spectral energy distribution (SED): if more luminous objects have a softer UV/X-ray spectra, then ionisation and photoelectric heating of the gas in the BLR would be reduced (e.g., Korista et al. 1998). An anti-correlation between the EW and the luminosity was found for the iron $K\alpha$ line in the X-ray band by Iwasawa & Taniguchi (1993, $EW \propto L^{-0.20}$), and it is usually dubbed the *X-ray Baldwin effect* or the *Iwasawa-Taniguchi effect*. Recent studies performed with the highest available spectral energy resolution of *Chandra*/HEG have shown that the X-ray Baldwin effect is mostly related to the narrow component of the Fe $K\alpha$ line, peaking at 6.4 keV (e.g., Shu et al. 2010). This component is thought to arise in the molecular torus, although a contribution from the BLR (e.g., Bianchi et al. 2008) or from the outer part of the disk (e.g., Petrucci et al. 2002) cannot

be completely ruled out. The X-ray Baldwin effect has been often explained as being due to the decrease of the covering factor of the torus with the luminosity (e.g., Page et al. 2004, Bianchi et al. 2007), in the frame of the so-called luminosity-dependent unification models (e.g., Ueda et al. 2003). In a recent paper (Ricci et al. 2013) we have shown that a luminosity-dependent covering factor of the torus is able to explain the slope of the X-ray Baldwin effect for equatorial column density of the torus $N_{\text{H}}^{\text{T}} \gtrsim 10^{23.1} \text{ cm}^{-2}$. Other possible explanations proposed are the delayed response of the re-processing material with respect to the variability of the primary continuum (Jiang et al. 2006; Shu et al. 2012), or a change in the ionisation state of the iron-emitting material with the luminosity (Nandra et al. 1997; Nayakshin 2000).

Studying a large sample of unabsorbed AGN, Bianchi et al. (2007) found a highly significant anti-correlation also between the Fe $K\alpha$ EW and the Eddington ratio ($\lambda_{\text{Edd}} = L_{\text{Bol}}/L_{\text{Edd}}$, where $L_{\text{Edd}} = 1.2 \times 10^{38} (M_{\text{BH}}/M_{\odot}) \text{ erg s}^{-1}$). Bianchi et al. (2007) found $EW \propto \lambda_{\text{Edd}}^{-0.19}$, i.e. an index similar to that obtained considering the X-ray luminosity, which leaves open the possibility that the Eddington ratio could play a significant role in the X-ray Baldwin effect. Winter et al. (2009) found that the Fe $K\alpha$ EW is more strongly correlated to λ_{Edd} than to the luminosity. However, in their work they used both unabsorbed and absorbed AGN, which might add confusion to the relation, as the EW of significantly obscured ($N_{\text{H}} > 10^{23} \text{ cm}^{-2}$) AGN is enhanced by the depletion of the con-

* E-mail: ricci@kusastro.kyoto-u.ac.jp

tinuum caused by the absorbing material in the line of sight. In a recent study of *Chandra*/HEG unabsorbed AGN, Shu et al. (2010), using the ratio between the 2–10 keV and the Eddington luminosity L_{2-10}/L_{Edd} as a proxy of λ_{Edd} (equivalent to assuming a constant bolometric correction), found that $EW \propto (L_{2-10}/L_{\text{Edd}})^{-0.20}$. They also found that, similarly to what has been obtained with the luminosity, the correlation is weaker ($EW \propto (L_{2-10}/L_{\text{Edd}})^{-0.11}$) when one considers values of L_{2-10}/L_{Edd} and EW averaged over different observations (*fit per source*) rather than using all the available observations for every object of the sample (*fit per observation*). In Table 1 we report the results of the most recent studies of the $EW - \lambda_{\text{Edd}}$ relation.

The first hint of the existence of an anti-correlation between the photon index Γ and the full width half-maximum (FWHM) of H β was found in the 0.1–2.4 keV energy band by Boller et al. (1996) studying a sample of narrow-line Seyfert 1s with *ROSAT*. This trend was later confirmed using *ASCA* observations at higher energies (e.g., Brandt et al. 1997, Reeves & Turner 2000), and Brandt & Boller (1998) hypothesised that it might be related to the dependence of both FWHM(H β) and Γ on λ_{Edd} . A significant positive correlation between Γ and λ_{Edd} was later found by several works performed using *ASCA*, *ROSAT*, *Swift* and *XMM-Newton* (e.g., Wang et al. 2004, Grupe 2004, Porquet et al. 2004b, Bian 2005, Grupe et al. 2010). The degeneracy between the dependence of Γ on FWHM(H β) and on λ_{Edd} was broken by Shemmer et al. (2006, 2008), who found that λ_{Edd} seems to be the main driver of the correlation. Shemmer et al. (2008), using estimates of M_{BH} obtained using H β , found that the relation between Γ and λ_{Edd} can be approximated by

$$\Gamma \simeq 0.31 \log \lambda_{\text{Edd}} + 2.11, \quad (1)$$

consistently with what was obtained by Wang et al. (2004) and by Kelly et al. (2007). A steeper relation between Γ and λ_{Edd} ($\Gamma \propto 0.60 \log \lambda_{\text{Edd}}$) has been found by Risaliti et al. (2009) and Jin et al. (2012). The relation between Γ and λ_{Edd} implies the existence of a strong link between the properties of the accretion flow and those of the warm corona. The fact that objects with higher values of λ_{Edd} show steeper photon indices has been explained by several authors as being due to a more efficient cooling of the corona caused by the larger optical/UV flux emitted by the accreting disk (e.g., Shemmer et al. 2008). This behaviour of Γ is similar to what has been observed in stellar mass black holes (Remillard & McClintock 2006), in agreement with the unification of accretion onto black holes across the mass scale.

The positive $\Gamma - \lambda_{\text{Edd}}$ correlation might play a role on the X-ray Baldwin effect. Objects with lower values of λ_{Edd} have a flatter continuum, which implies that the amount of photons that can produce the fluorescent Fe K α emission is larger, which would produce a larger EW. The opposite would happen for objects at high Eddington ratios, which would create an anti-correlation between EW and λ_{Edd} . If the EW of the iron K α line is mainly correlated to λ_{Edd} , the relation between Γ and λ_{Edd} could also be, at least in part, responsible for the observed trend. In this work we aim at constraining the effect of the $\Gamma - \lambda_{\text{Edd}}$ correlation on the EW of the iron K α line for different geometries. We simulate the spectra of unabsorbed populations of AGN considering three different geometries for the reflecting material (spherical-toroidal, toroidal and slab), and we study the relation between the EW of the iron K α line and the Eddington ratio. We consider only unabsorbed AGN to compare our results to the most reliable studies of the X-ray Baldwin effect.

The paper is organised as follows. In Sect. 2 we study the

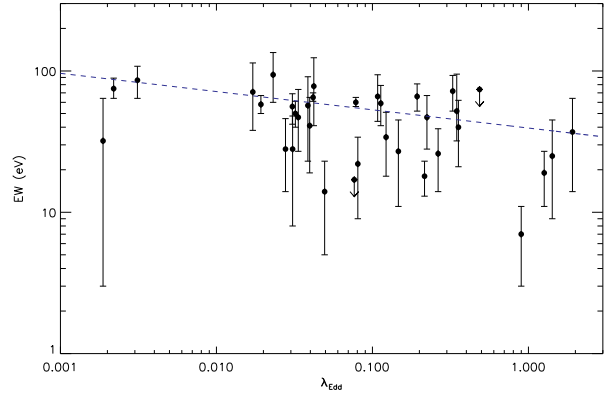


Figure 1. Equivalent width of the narrow component of the iron K α line versus the Eddington ratio for the objects of the *Chandra*/HEG sample of Shu et al. (2010). The values of the Eddington ratio were calculated using bolometric corrections obtained from the SED (Table 2). The dashed line represents the best fit to the data ($B = -0.13 \pm 0.03$, Table 1).

Table 1. Summary of the most recent studies of the $EW - \lambda_{\text{Edd}}$ relation. The model commonly used to fit the data is $\log EW = A + B \log \lambda_{\text{Edd}}$, where $\lambda_{\text{Edd}} = L_{\text{Bol}}/L_{\text{Edd}}$. The table lists separately works for which the fit was done *per observation* (i.e. using all the available observations for every source of the sample) and *per source* (i.e. averaging the values of EW and λ_{Edd} of different observations of the same source). The table shows (1) the reference, (2) the value of the slope, (3) the number and the type (radio-quiet, RQ, or radio-loud, RL) of objects of the sample, and (4) the observatory and instrument used.

(1)	(2)	(3)	(4)
Reference	B	Sample	Observatory/instrument
Fits per Observation			
Shu et al. 2010 ¹	-0.20 ± 0.03	33 (RQ+RL)	<i>Chandra</i> /HEG
Bianchi et al. 2007 ²	-0.19 ± 0.05	82 (RQ)	<i>XMM-Newton</i> /EPIC
Bianchi et al. 2007 ¹	-0.16 ± 0.06	82 (RQ)	<i>XMM-Newton</i> /EPIC
Fits per Source			
Shu et al. 2010 ¹	-0.11 ± 0.04	33 (RQ+RL)	<i>Chandra</i> /HEG
This work ³	-0.13 ± 0.03	33 (RQ+RL)	<i>Chandra</i> /HEG
This work ^{3,A}	-0.18 ± 0.05	33 (RQ+RL)	<i>Chandra</i> /HEG

Notes: ¹ constant bolometric correction; ² luminosity-dependent bolometric; corrections of Marconi et al. (2004); ³ using the average bolometric corrections calculated directly from the AGN bolometric emission (see Sect. 2);

^A taking into account the errors on λ_{Edd} .

relation between EW and λ_{Edd} using the *Chandra*/HEG data of Shu et al. (2010) and the bolometric corrections obtained from studies of the AGN spectral energy distribution. In Sect. 3 we present our simulations for a toroidal (3.1), a spherical toroidal (3.2) and a slab (3.3) geometry, we discuss the influence of scatter (3.4) and of the underlying λ_{Edd} distribution (3.5). In Sect. 4 we study the relation between the narrow Fe K α EW and the photon index using the *Chandra* sample of Shu et al. (2010) and the *Suzaku* sample of Fukazawa et al. (2011). In Sect. 5 we discuss our results, and in Sect. 6 we present our conclusions.

Table 2. The table reports (1) the equivalent width of the narrow component of the iron $K\alpha$ line, (2) the 2–10 keV luminosity, (3) the black hole mass, (4) the method used for calculating the black hole mass, (5) the 2–10 keV average bolometric correction, (6) the bolometric luminosity, and (7) the Eddington ratio for the objects in the sample of Shu et al. (2010). The values of (1) and (2) were taken from Shu et al. (2010) averaging when possible different observations. For the objects for which no value of the 2–10 keV bolometric correction was available we fixed $\kappa_x = 20$.

Source	(1) EW [eV]	(2) L_{2-10} [10^{43} erg s $^{-1}$]	(3) $\log(M_{\text{BH}}/M_{\odot})$	(4) Method	(5) κ_x	(6) $\log L_{\text{Bol}}$ [erg s $^{-1}$]	(7) λ_{Edd}
Fairall 9	47 $^{+27}_{-20}$	11.6	8.41 \pm 0.09 ^a	RM	8.9 \pm 0.7	45.0	0.033
NGC 526a	28 $^{+20}_{-20}$	2.4	7.9 \pm 0.1 ^b	KB	13.1 \pm 0.9	44.5	0.031
Mrk 590	78 $^{+46}_{-37}$	1.3	7.68 \pm 0.08 ^a	RM	18.6 \pm 1.1	44.4	0.042
NGC 985	57 $^{+34}_{-34}$	4.4	8.4 \pm 0.1 ^b	KB	24.1 \pm 1.3	45.0	0.039
ESO 198–G24	71 $^{+43}_{-33}$	3.1	8.5 \pm 0.5 ^c	ER	20*	44.8	0.017
3C 120	47 $^{+20}_{-19}$	11.7	7.7 \pm 0.2 ^a	RM	12.6 \pm 0.4	45.2	0.22
NGC 2110	75 $^{+14}_{-11}$	0.51	8.3 \pm 0.3 ^d	VD	10.3 \pm 0.7	43.7	0.0022
PG 0844+349	52 $^{+43}_{-20}$	5.4	8.0 \pm 0.2 ^a	RM	72 \pm 8	45.6	0.35
Mrk 705	26 $^{+48}_{-26}$	2.6	7.0 \pm 0.1 ^e	ER	20*	44.7	0.49
MCG –5–23–16	50 $^{+11}_{-10}$	1.6	7.9 \pm 0.4 ^c	VD	20*	44.5	0.032
NGC 3227	32 $^{+32}_{-29}$	0.08	7.6 \pm 0.2 ^a	RM	12.0 \pm 0.5	43.0	0.0019
NGC 3516	58 $^{+9}_{-8}$	0.70	7.6 \pm 0.1 ^a	RM	14.1 \pm 1.6	44.0	0.019
NGC 3783	60 $^{+5}_{-4}$	1.4	7.47 \pm 0.09 ^a	RM	19.8 \pm 0.9	44.4	0.078
NGC 4051	94 $^{+41}_{-34}$	0.02	6.3 \pm 0.2 ^a	RM	26.4 \pm 1.1	42.7	0.023
NGC 4151	65 $^{+5}_{-4}$	0.36	7.1 \pm 0.1 ^a	RM	18 \pm 2	43.8	0.042
Mrk 766	37 $^{+27}_{-23}$	0.86	6.3 \pm 0.4 ^c	RM	45 \pm 3	44.6	1.92
3C 273	7 $^{+4}_{-4}$	654	8.95 \pm 0.07 ^a	RM	15 \pm 3	47.0	0.90
NGC 4593	59 $^{+20}_{-18}$	0.81	6.7 \pm 0.6 ^a	RM	9.0 \pm 0.5	43.9	0.11
MCG –6–30–15	18 $^{+5}_{-5}$	0.59	6.7 \pm 0.2 ^d	VD	22.0 \pm 1.0	44.1	0.22
IRAS 13349+2438	40 $^{+22}_{-19}$	10.7	7.7 \pm 0.5 ^c	ER	20*	45.3	0.36
IC 4329A	19 $^{+8}_{-8}$	10.1	7.0 \pm 0.8 ^a	RM	15.0 \pm 1.0	45.2	1.26
Mrk 279	66 $^{+28}_{-22}$	2.9	7.5 \pm 0.1 ^a	RM	15.5 \pm 0.3	44.7	0.11
NGC 5506	66 $^{+15}_{-14}$	0.55	6.6 \pm 0.5 ^f	VD	16.8 \pm 1.2	44.0	0.19
NGC 5548	56 $^{+13}_{-14}$	1.9	7.83 \pm 0.03 ^a	RM	13.1 \pm 1.5	44.4	0.031
Mrk 290	27 $^{+18}_{-16}$	3.2	7.39 \pm 0.07 ^g	RM	13.5 \pm 0.9	44.6	0.15
PDS 456	4 $^{+13}_{-4}$	37.3	8.9 \pm 0.5 ^h	ER	20*	45.9	0.08
E1821+643	26 $^{+13}_{-12}$	362.5	9.4 \pm 0.5 ^h	ER	20*	46.9	0.26
3C 382	14 $^{+9}_{-9}$	40.6	8.8 \pm 0.5 ^h	ER	10.1 \pm 0.6	45.6	0.049
IRAS 18325–5926	5 $^{+9}_{-5}$	2.3	–	–	20*	44.7	–
4C +74.26	28 $^{+18}_{-14}$	66.2	9.6 \pm 0.5 ^d	ER	20*	46.1	0.028
Mrk 509	34 $^{+17}_{-16}$	15.6	8.16 \pm 0.03 ^a	RM	13.6 \pm 0.6	45.3	0.12
NGC 7213	86 $^{+22}_{-22}$	0.18	8.0 \pm 0.3 ⁱ	VD	20.3 \pm 1.6	43.6	0.0031
NGC 7314	41 $^{+24}_{-22}$	0.17	6.1 \pm 0.1 ^b	KB	3.9 \pm 0.4	42.8	0.040
Ark 564	25 $^{+20}_{-16}$	3.7	6.3 \pm 0.5 ^c	ER	9.2 \pm 3.7	44.5	1.42
MR 2251–178	22 $^{+12}_{-13}$	25.3	8.8 ^j	KB	22.0 \pm 0.3	45.8	0.081
NGC 7469	72 $^{+21}_{-20}$	1.5	7.09 \pm 0.05 ^a	RM	32.2 \pm 1.3	44.7	0.33

Notes. The values of the M_{BH} were taken from: ^a Peterson et al. (2004), ^b Vasudevan et al. (2010), ^c De Marco et al. (2013), ^d Beckmann et al. (2009), ^e Vestergaard (2002), ^f Middleton et al. (2008), ^g Denney et al. (2010), ^h Wang et al. (2009), ⁱ Woo & Urry (2002), ^j Winter et al. (2009). The methods used for the mass calculation are: reverberation mapping (RM), K-band host bulge luminosity (KB), empirical $L(5100\text{\AA})$ vs R_{BLR} relation (ER), and stellar velocity dispersion (VD).

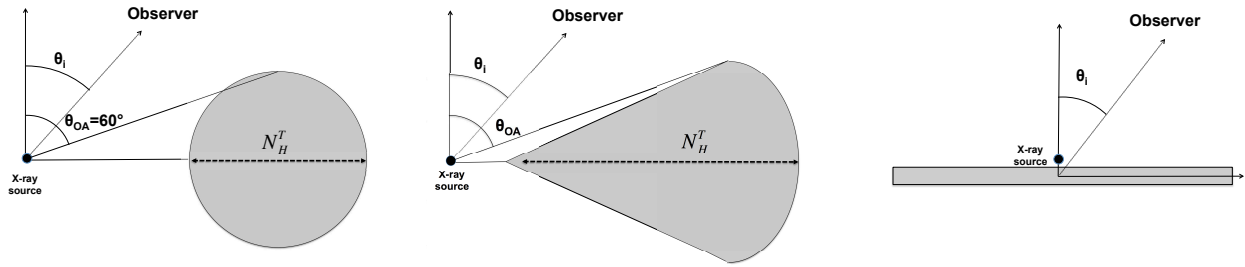


Figure 2. Schematic representation of the toroidal (*left panel*), spherical-toroidal (*central panel*) and slab (*right panel*) geometries. In all cases θ_i is the inclination angle of the observer. In the toroidal geometry the half-opening angle θ_{OA} is set to 60° , while in the spherical-toroidal geometry it varies between 10° and 70° . In both the toroidal and spherical-toroidal geometry the equatorial column density of the torus N_H^T spans between $10^{22.5}$ and 10^{25} cm^{-2} .

2 THE $EW - \lambda_{\text{Edd}}$ RELATION

The studies of the $EW - \lambda_{\text{Edd}}$ relation performed so far have used either constant (e.g., Shu et al. 2010, Bianchi et al. 2007) or luminosity-dependent (e.g., Marconi et al. 2004, Bianchi et al. 2007) 2–10 keV bolometric corrections (κ_x , where $L_{\text{Bol}} = \kappa_x \cdot L_{2-10}$). It has been however shown that the value of κ_x does not have a clear dependence on the bolometric luminosity (e.g., Vasudevan & Fabian 2007, Marchese et al. 2012), while it appears to be connected to the Eddington ratio (Vasudevan & Fabian 2007).

In order to better constrain the slope of the $EW - \lambda_{\text{Edd}}$ we used the *per source* values of EW and L_{2-10} reported by the *Chandra*/HEG study of Shu et al. (2010) (where the line width was fixed to $\sigma = 1 \text{ eV}$ to consider only the narrow component), together with the best estimates of the black-hole masses of their samples reported in the literature. For 18 sources values of M_{BH} obtained by reverberation mapping were available (e.g., Peterson et al. 2004), while for the rest of the sources we used values obtained by i) the K-band host bulge luminosity- M_{BH} relation (e.g., Vasudevan et al. 2010), ii) the empirical $L(5100\text{\AA})$ vs R_{BLR} relation (e.g., Vestergaard 2002), iii) the stellar velocity dispersion (e.g., Woo & Urry 2002). We took the values of κ_x obtained directly from studies of the bolometric AGN emission performed by Vasudevan & Fabian (2007), Vasudevan et al. (2009), Vasudevan & Fabian (2009), and Vasudevan et al. (2010), averaging the values when several were available. For the eight sources of the sample for which no value of κ_x was available we fixed $\kappa_x = 20$ (Vasudevan & Fabian 2009). The values of λ_{Edd} for the *Chandra*/HEG sample are reported in Table 2. We fitted the data using

$$\log EW = A + B \log \lambda_{\text{Edd}}. \quad (2)$$

The scatter plot of EW versus λ_{Edd} and the fit to the data are shown in Fig. 1. We found that using the measured bolometric correction the slope of $EW - \lambda_{\text{Edd}}$ is consistent ($B = -0.13 \pm 0.03$) with the value obtained using constant values of κ_x (see Table 1). Using the `fitexy` procedure (Press et al. 1992), which allows to take into account also the uncertainties of λ_{Edd} , we obtained a steeper slope ($B = -0.18 \pm 0.05$). The correlation yields a null-hypothesis probability of $P_n \sim 1\%$ and the Spearman’s rank correlation coefficient is $\rho = -0.44$. Interestingly, the decrease of the EW with the X-ray luminosity is more significant ($P_n \sim 0.03\%$, $\rho = -0.64$). Considering only the objects for which it was possible to estimate κ_x does not increase the significance of the correlation.

3 SIMULATIONS

In order to simulate the $EW - \lambda_{\text{Edd}}$ relation produced by the dependence of Γ on λ_{Edd} , we followed what we have done in Ricci et al. (2013) to study the influence of the decrease of the covering factor of the torus with the luminosity on the X-ray Baldwin effect. We initially considered an uniform distribution of Eddington ratios, with λ_{Edd} spanning between 0.01 and 1, with a binning of $\Delta \lambda_{\text{Edd}} = 0.01$. For each value of λ_{Edd} we determined the photon index using the relation of Shemmer et al. (2008, Eq. 1), and simulated in XSPEC 12.7.1 (Arnaud 1996) a large number of spectra, using Monte Carlo simulations of reflected X-ray radiation. These simulations were carried out to examine the shape of the reflected emission for a given X-ray continuum, and assume three different geometries of the reprocessing material (Fig. 2): toroidal (Sect. 3.1), spherical-toroidal (Sect. 3.2) and slab (Sect. 3.3). For each geometry we explored the parameter space and created synthetic unabsorbed populations. In XSPEC we measured the value EW of the simulated spectra, using for the continuum the same models as those used for the simulations and a Gaussian line for the iron $K\alpha$ line. We then studied the relation of EW with the Eddington ratio fitting the values of the synthetic populations with Eq. 2 using the weighted least-square method. The weights used are $w = \sin \theta_i$, where θ_i is the inclination angle of the observer. This is done to take into account the non-uniform probability of randomly observing the AGN within a certain solid angle from the polar axis. In Sect. 3.4 we study the influence of scatter in the $\Gamma - \lambda_{\text{Edd}}$ relation, and in Sect. 3.5 we assume more realistic λ_{Edd} distributions. In Sect. 5 we discuss the impact of a steeper $\Gamma - \lambda_{\text{Edd}}$ trend, as that found by Risaliti et al. (2009), on our simulations. Throughout the paper we assume solar metallicities.

3.1 Toroidal geometry

Murphy & Yaqoob (2009) carried out Monte-Carlo calculations of Green’s functions to study the reprocessed features originated in a toroidal geometry (see left panel of Fig. 2). These simulations are part of a X-ray spectral fitting model (`MYTorus`¹), which can be implemented in XSPEC as a combination of three table models. These table models include the zeroth-order continuum, the scattered continuum and a component which contains the fluorescent lines. The main parameters of `MYTorus` are the photon index Γ , the equatorial column density of the torus N_H^T and the inclination angle

¹ <http://www.mytorus.com/>

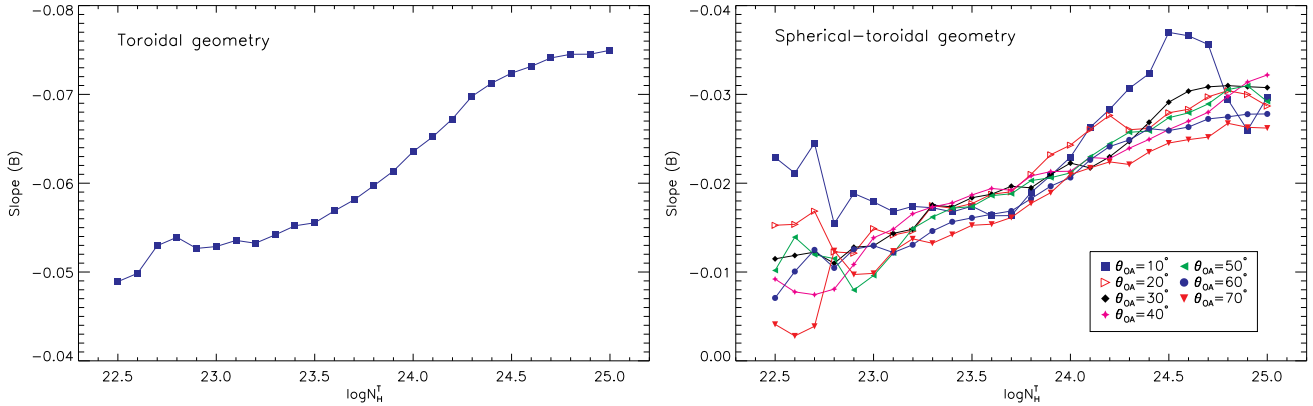


Figure 3. Slopes of $EW - \lambda_{\text{Edd}}$ trend obtained simulating a population of unabsorbed AGN with photon indices increasing with the Eddington ratio as predicted by Eq. 1 for equatorial column densities of the torus between $10^{22.5} \text{ cm}^{-2}$ and 10^{25} cm^{-2} . The geometry considered here are toroidal (*left panel*) and spherical-toroidal (*right panel*).

of the observer θ_i . In MYTorus the half-opening angle of the torus θ_{OA} is fixed to 60° , while θ_i can vary between 0° and 90° , and N_{H}^{T} between 10^{22} cm^{-2} and 10^{25} cm^{-2} . The fluorescent emission lines in MYTorus are convolved with a Gaussian function (gsmooth in XSPEC) to take into account the velocity broadening. The width of the Gaussian broadening is

$$\sigma_{\text{E}} = \sigma_{\text{L}} \left(\frac{E}{6 \text{ keV}} \right)^{\alpha}, \quad (3)$$

where

$$\sigma_{\text{L}} = 0.850 \left(\frac{V_{\text{FWHM}}}{100 \text{ km s}^{-1}} \right) \text{ eV}. \quad (4)$$

We used $\text{FWHM} = 2000 \text{ km s}^{-1}$, as obtained by recent *Chandra*/HEG observations of unobscured AGN (Shu et al. 2010), which is equivalent to $\sigma_{\text{L}} = 17 \text{ eV}$, and $\alpha = 1$. MYTorus does not allow a cut-off power law, but considers a *termination energy* (E_{T}). As the choice of E_{T} does not affect significantly the values of the EW of the iron $K\alpha$ line, we arbitrarily chose $E_{\text{T}} = 500 \text{ keV}$. We used a model which includes the three components implemented in MYTorus², and fixed the value of the normalisation of the scattered continuum (which includes the Compton hump) and of the fluorescent-line model to that of the zeroth-order continuum. We considered 26 values of equatorial column densities between $\log N_{\text{H}}^{\text{T}} = 22.5$ and $\log N_{\text{H}}^{\text{T}} = 25$, with a binning of $\Delta \log N_{\text{H}}^{\text{T}} = 0.1$. For each value of N_{H}^{T} we simulated a population of unabsorbed AGN, with $0^\circ \leq \theta_i < \theta_{\text{OA}}$, with a binning of $\Delta \theta_i = 3^\circ$, and with Γ following Eq. 1.

After extracting the values of EW we fitted the obtained $EW(\lambda_{\text{Edd}})$ trend with Eq. 1 for each synthetic population, and obtained values of the slope that vary between $B \simeq -0.05$ (for $\log N_{\text{H}}^{\text{T}} = 22.5$) and $B \simeq -0.075$ (for $\log N_{\text{H}}^{\text{T}} = 25$). The variation of B with N_{H}^{T} is shown in the left panel of Fig. 3.

3.2 Spherical-toroidal geometry

Monte-Carlo simulations of the reprocessed radiation considering a spherical-toroidal geometry have been presented by Ikeda et al.

² In XSPEC the model was `pow*etable{mytorus_Ezero_v00.fits}+atable{mytorus_scatteredH500_v00.fits}+gsmooth(atable{mytL_V0000010nEp000H500_v00.fits})`

(2009). These simulations are also stored in tables, so that they can be used for spectral fitting as in the case of MYTorus. The angles in this model are the same as those of the toroidal geometry (see central panel of Fig. 2 or Fig. 1 in Ricci et al. 2013). The model of Ikeda et al. (2009) has the advantage, with respect to MYTorus, of having a variable half-opening angle of the torus θ_{OA} . The other parameters of this model are θ_i , Γ and N_{H}^{T} , similarly to MYTorus, although the values of θ_i allowed are in a slightly different range ($1^\circ - 89^\circ$). In the model the energy of the cutoff is fixed to $E_{\text{C}} = 360 \text{ keV}$. We simulated an unabsorbed population of AGN for each value of θ_{OA} and $\log N_{\text{H}}^{\text{T}}$, using values of θ_i between 1° and θ_{OA} with a binning of $\Delta \theta_i = 3^\circ$, and the photon index varying according to Eq. 1. We selected 7 different values of θ_{OA} , from 10° to 70° , with $\Delta \theta_{\text{OA}} = 10^\circ$, and 26 values of N_{H}^{T} , from $\log N_{\text{H}}^{\text{T}} = 22.5$ to $\log N_{\text{H}}^{\text{T}} = 25$, with $\Delta \log N_{\text{H}}^{\text{T}} = 0.1$.

The values of B obtained fitting with Eq. 1 the synthetic populations are shown in the right panel of Fig. 3, and vary between $B \simeq -0.003$ (for $\theta_{\text{OA}} = 70^\circ$ and $\log N_{\text{H}}^{\text{T}} = 22.6$) and $B \simeq -0.037$ (for $\theta_{\text{OA}} = 10^\circ$ and $\log N_{\text{H}}^{\text{T}} = 24.5$).

3.3 Slab geometry

For the sake of completeness we investigated also the impact of the $\Gamma - \lambda_{\text{Edd}}$ relation on the Fe $K\alpha$ line EW using a slab geometry (right panel of Fig. 2), commonly used to reproduce the reflection of the X-ray continuum on the accretion disk. We used the `pexmon` model (Nandra 2006), which is based on the spectral model for reflection on a semi-infinite slab of neutral material of Magdziarz & Zdziarski (1995, `pexrav`), linking to the reflection fraction R the EW of the iron $K\alpha$ line. The parameter R is defined as the strength of the reflection component relative to that expected from a slab subtending 2π solid angle ($R = 2\pi/\Omega$). The strength of the Fe $K\alpha$ line in `pexmon` is determined using the Monte-Carlo calculations of George & Fabian (1991). In the model the relation between EW and Γ is parametrised as

$$EW = 9.66 EW_0 (\Gamma^{-2.8} - 0.56), \quad (5)$$

where $EW_0 = 144 \text{ eV}$ is the equivalent width for a face-on slab ($\theta_i = 0^\circ$), considering $\Gamma = 1.9$ and iron abundance relative to hydrogen of 3.31×10^{-5} (Anders & Ebihara 1982). We simulated populations of unabsorbed AGN for five different values of the reflection parameter ($R = 0.2, 0.4, 0.6, 0.8, 1$), using the same θ_i distribu-

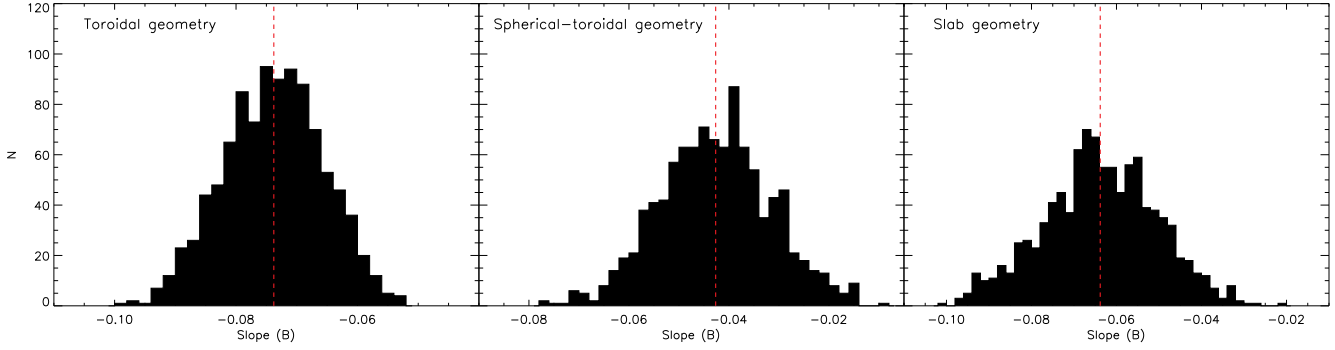


Figure 4. Histograms of the values of the slope of the $EW - \lambda_{\text{Edd}}$ relation obtained by performing 1,000 MonteCarlo simulations for the different geometries of the reflecting material described in Sects. 3.1-3.3, including a scatter of $\Delta\Gamma \sim 0.1\Gamma$ in the $\Gamma - \lambda_{\text{Edd}}$ relation (Eq. 1) and considering random values of θ_i . For the toroidal geometry $\theta_{\text{OA}} = 60^\circ$, $N_{\text{H}}^{\text{T}} = 10^{25} \text{ cm}^{-2}$ (left panel), for the spherical-toroidal geometry $\theta_{\text{OA}} = 10^\circ$, and $N_{\text{H}}^{\text{T}} = 10^{24.5} \text{ cm}^{-2}$ (central panel), and for the slab geometry $R = 1$ (right panel). The vertical dotted lines represent the average values of the slope.

tion we have used for MYTorus ($\theta_i < 60^\circ$). The energy of the cutoff does not play a significant role on the EW of the Fe $K\alpha$ line, and it was fixed to $E_C = 500 \text{ keV}$. In the slab model the value of N_{H} of the reflecting material is fixed to infinite, so that we cannot vary it.

Fitting the simulated data we obtain that the value of the slope does not vary significantly for different values of R , and is $B \approx -0.058$.

3.4 The effects of scatter in the $\Gamma - \lambda_{\text{Edd}}$ relation

The values of the slopes obtained in the previous sections for different geometries of the reflector have been calculated neglecting the significant scatter found in the $\Gamma - \lambda_{\text{Edd}}$ relation ($\Delta\Gamma \sim 0.1\Gamma$, Shemmer et al. 2008). In order to account for this scatter, for each of the three geometries, and considering the set of parameters for which slope was the steepest, we carried out 1,000 Monte-Carlo simulations. In these simulations, for each value of λ_{Edd} the photon index had a random scatter within $\Delta\Gamma \sim 0.1\Gamma$. The inclination angle was randomly selected, in order to simulate unabsorbed AGN, between 1° and θ_{OA} for the spherical-toroidal geometry, and between 0° and 60° for the remaining two geometries. For each simulation we calculated the value of B using Eq. 2 as described in Sect. 3.

For the toroidal geometry ($\theta_{\text{OA}} = 60^\circ$, $N_{\text{H}}^{\text{T}} = 10^{25} \text{ cm}^{-2}$) the average slope is $B = -0.074$ and the standard deviation $\sigma_B = 0.008$ (left panel of Fig. 4), for the spherical-toroidal geometry ($\theta_{\text{OA}} = 10^\circ$, $N_{\text{H}}^{\text{T}} = 10^{24.5} \text{ cm}^{-2}$) the average slope is $B = -0.043$ and the standard deviation $\sigma_B = 0.011$ (central panel of Fig. 4), while for the slab geometry the average slope we obtained is $B = -0.064$ and the standard deviation $\sigma_B = 0.013$. None of the Monte-Carlo runs produce values of B consistent with the slope of the X-ray Baldwin effect we found in Sect. 2 (see also Table 1).

3.5 Assuming a realistic λ_{Edd} distribution

The simulations discussed so far have been carried out assuming an unrealistic uniform λ_{Edd} distribution for the synthetic AGN populations. In order to account for a realistic distribution of λ_{Edd} we used the 9-months *Swift*/BAT AGN sample. We took the values of the 2–10 keV luminosity and of M_{BH} reported in the X-ray study of Winter et al. (2009). We assumed a constant 2–10 keV bolometric correction of $\kappa_x = 20$, and took into account the 52 objects with $\log \lambda_{\text{Edd}} \geq -2$. For each geometry we used the set of parameters for which the steepest slope B was obtained (see Sect. 3.1-

3.3), and ran 1,000 Monte-Carlo simulations using Eq. 1 to obtain Γ , and assuming a random inclination angle between 1° and θ_{OA} for the spherical-toroidal geometry, and between 0° and 60° for the remaining two geometries. We obtained an average value of $B = -0.080$ with a standard deviation of $\sigma_B = 0.005$ for the toroidal geometry, while $B = -0.048$ with $\sigma_B = 0.015$ for the spherical-toroidal geometry, and $B = -0.051$ with $\sigma_B = 0.016$ for the slab geometry.

To account for the possible error introduced by using constant bolometric corrections we considered the results reported by Vasudevan et al. (2010) for the 9-months *Swift*/BAT AGN sample. In their work they calculated the values of κ_x using the *Swift*/BAT and *IRAS* fluxes together with the AGN nuclear SED templates of Silva et al. (2004). We considered only the 28 unobscured AGN for which the values of κ_x were available, in order to have a sample consistent with those usually used for studies of the X-ray Baldwin effect. Following what we did for the sample of Winter et al. (2009), we obtained from our simulations an average value of $B = -0.084$ with a standard deviation of $\sigma_B = 0.009$ for the toroidal geometry, $B = -0.037$ with $\sigma_B = 0.032$ for the spherical-toroidal geometry, and $B = -0.050$ with $\sigma_B = 0.033$ for the slab geometry. The larger dispersion associated with these simulations with respect to those performed using the sample of Winter et al. (2009) is likely related to the lower number of objects we used. Due to the larger scatter obtained, for the toroidal geometry $\sim 3\%$ of the of the Monte-Carlo runs produces values of B consistent within 1σ with *Chandra*/HEG observations, $\sim 2\%$ for the spherical-toroidal geometry and $\sim 7\%$ for the slab geometry.

As a last test we used the Eddington ratio distribution obtained from the Hamburg/ESO survey of type-I low-redshift ($z < 0.3$) AGN by Schulze & Wisotzki (2010). In their work they found that, after correcting for observational biases, the intrinsic λ_{Edd} distribution of unobscured AGN can be well represented by a log-normal distribution with a mean of $\log \lambda_{\text{Edd}} = -1.83$ and a standard deviation of $\sigma_\lambda = 0.49$. Generating random values of λ_{Edd} distributed with a log-normal distribution (for $\log \lambda_{\text{Edd}} > -2$) with the parameters found by Schulze & Wisotzki (2010), we created a dummy AGN population of 100 sources. We used this population to perform 1,000 Monte-Carlo simulations following what we did for the samples of Winter et al. (2009) and Vasudevan et al. (2010). We obtained an average value of $B = -0.090$ with a standard deviation of $\sigma_B = 0.008$ for the toroidal geometry, $B = -0.041$ with $\sigma_B = 0.028$ for the spherical-toroidal geometry, and $B = -0.040$

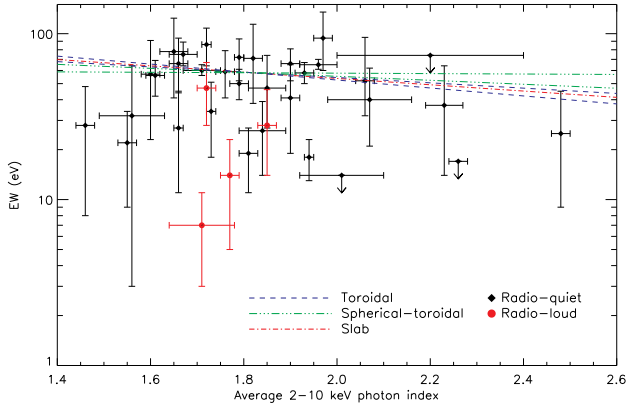


Figure 5. Scatter plot of the EW of the narrow component of the iron $K\alpha$ line versus the photon index for the *Chandra*/HEG sample. The values of EW are those reported in Shu et al. (2010) fixing $\sigma = 1$ eV and averaging when possible different observations of the same source. The values of Γ were taken from the literature (see Appendix A), averaging all the results of the last ~ 10 years obtained with *Chandra*, *XMM-Newton* and *Suzaku*. The lines represent the $EW - \Gamma$ trends expected considering three different geometries of the reprocessing material: toroidal (blue dashed lines), spherical-toroidal (green dot-dot-dashed line) and slab (red dot-dashed line). The values of α were obtained fitting the *Chandra*/HEG data, fixing β to the results of the simulations (see Eq. 6). For the toroidal and the spherical-toroidal geometries the values of β used are the maximum and minimum obtained by the simulations.

with $\sigma_B = 0.030$ for the slab geometry. For the toroidal geometry $\sim 12\%$ of the simulations produce values of B consistent with the observations, while lower percentages are obtained for the spherical-toroidal ($\sim 3\%$) and slab ($\sim 2\%$) geometries.

4 THE RELATION BETWEEN THE IRON $K\alpha$ EW AND Γ

So far we have discussed the influence of the dependence of Γ on λ_{Edd} on the X-ray Baldwin effect. In this section we investigate the relation between the narrow component of the Fe $K\alpha$ EW and the photon index. A clear trend between these two quantities might in fact suggest that the $\Gamma - \lambda_{\text{Edd}}$ correlation plays an important role in the observed $EW - \lambda_{\text{Edd}}$ relation. Using *ASCA* observations of 25 unabsorbed AGN, Lubiński & Zdziarski (2001) found evidence of a possible positive trend between the iron $K\alpha$ EW and Γ . A weak positive correlation was also found by Perola et al. (2002) studying *BeppoSAX* observations of bright AGN. A more complex relationship between these two quantities was found by the *RXTE* study of Mattson et al. (2007). In their study they analysed 350 time-resolved spectra of 12 type-I AGN, and found that the EW of the iron line is positively correlated with the photon index up to $\Gamma \approx 2$, where the trend turns over and the two parameters become anti-correlated. However, in all these studies the EW might also include the contribution of a broad component.

4.1 The *Chandra*/HEG sample

In order to study the relation between the narrow component of the iron $K\alpha$ line and the photon index we used the EW obtained by *Chandra*/HEG observations of a sample of 36 type-1/1.5 AGN (fixing $\sigma = 1$ eV) and reported in Shu et al. (2010). To reduce the

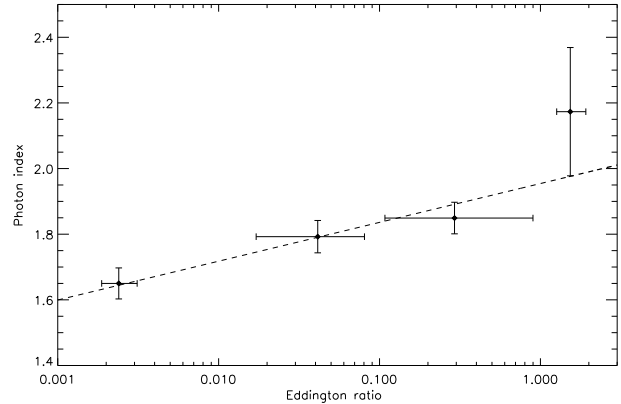


Figure 6. Rebinned scatter plot of the photon index versus the Eddington ratio of the *Chandra*/HEG type-I AGN sample of Shu et al. (2010). The dashed line represents the best fit to the data ($\Gamma \propto 0.12 \log \lambda_{\text{Edd}}$).

effects of variability of the primary continuum, we used the values of EW averaged, when possible, over several observations. We collected the values of Γ from *XMM-Newton*, *Chandra* and *Suzaku* studies of the sources performed in the last ten years (see Appendix A), and used the average of all the observations, in order to reduce the impact of photon-index variability. The material responsible for the narrow component of the Fe $K\alpha$ line is in fact thought to be located at several light years from the central engine, so that the response of the line to changes of Γ is not simultaneous. The scatter plot of the EW of the narrow component of the iron $K\alpha$ line versus the photon index is shown in Fig. 5. From the figure one can see that the data are dominated by scatter, and do not appear to be neither linearly correlated nor constant, with the Spearman's rank correlation coefficient being $\rho = -0.01$. Excluding the upper limits and fitting the data with a constant, one obtains $\chi^2 \approx 73$ for 32 degrees of freedom. Using the *fitxexy* procedure to fit the data with

$$\log EW = \alpha + \beta \Gamma, \quad (6)$$

we obtained $\alpha = 1.8 \pm 0.2$ and $\beta = -0.05 \pm 0.12$.

To compare the data to the expected $EW - \Gamma$ trend, we investigated the relation obtained by the three different geometries. This was done simulating, similarly to what was done in Sect. 3, several unabsorbed populations of AGN, with a uniform distribution of Γ between 1.5 and 2.5. We fitted the simulated data with Eq. 6, using the weighted least-square method, with the same weights we used for Eq. 2. In the case of the toroidal geometry β varies between -0.16 (for $\log N_{\text{H}}^{\text{T}} = 22.5$) and -0.23 (for $\log N_{\text{H}}^{\text{T}} = 25$). For the spherical toroidal geometry the values of β vary between -0.09 (for $\theta_{\text{OA}} = 70^\circ$ and $\log N_{\text{H}}^{\text{T}} = 22.6$) and -0.15 (for $\theta_{\text{OA}} = 10^\circ$ and $\log N_{\text{H}}^{\text{T}} = 24.5$), while for the slab geometry we obtained $\beta = -0.28$ (for $R = 1$). The expected trends are plotted in Fig. 5. Given the heterogeneous sampling of the values of Γ and the large scatter in the data, we cannot conclude whether the photon index plays a dominant role or not.

In Fig. 6 we plot the rebinned scatter plot of the photon index versus the Eddington ratio for the *Chandra*/HEG sample. Fitting the data with a log-linear function we obtained a dependence of Γ on $\log \lambda_{\text{Edd}}$ significantly weaker than the one found by Shemmer et al. (2008):

$$\Gamma = (1.95 \pm 0.06) + (0.12 \pm 0.04) \log \lambda_{\text{Edd}}. \quad (7)$$

However, the intrinsic correlation might at least in part be attenu-

ated by the fact that we considered values of Γ which were averaged over the last ~ 10 years, while the values of the Eddington ratio were obtained using only *Chandra*/HEG observations. The photon index is in fact expected to react on short time scales to changes of λ_{Edd} , so that our treatment is likely to introduce additional scatter to the correlation.

4.2 Reducing the effects of variability using *Suzaku* and *Swift*/BAT

In order to reduce the possible effects of variability we expanded our study using the *Suzaku* sample of Fukazawa et al. (2011) and the results of the 58-months 14–195 keV *Swift*/BAT catalog (Baumgartner et al. 2010). The flux of the continuum is more variable than that of the Fe $K\alpha$ line, and using the 58-months averaged 14–195 keV *Swift*/BAT flux (F_{BAT}) allows us to smooth out the effects of continuum variability. To have a proxy of the Fe $K\alpha$ EW less sensitive to variability we divided the flux of the iron $K\alpha$ line ($F_{K\alpha}$) obtained by *Suzaku* by F_{BAT} , and studied the relation of $F_{K\alpha}/F_{\text{BAT}}$ with the *Swift*/BAT photon index. Of the 87 AGN³ reported in the work of Fukazawa et al. (2011) we excluded the 13 Compton-thick Seyfert 2s because their BAT flux is likely to be significantly attenuated, the seven objects for which no iron $K\alpha$ line was detected by *Suzaku* and the four sources not detected by *Swift*/BAT. The final sample we used contained 63 AGN, of which 30 Seyfert 1s, 31 Seyfert 2s and 2 LINERs. For the 11 objects for which several *Suzaku* observations were reported we used the average values of the iron $K\alpha$ flux. In Fig. 7 the scatter plot of $F_{K\alpha}/F_{\text{BAT}}$ versus the *Swift*/BAT photon index is shown. Only a moderately significant positive correlation between the two quantities is found ($\rho = 0.3$, $P_n \sim 2\%$). We fitted the data with a linear relationship of the type $\log(F_{K\alpha}/F_{\text{BAT}}) = \xi + \mu\Gamma$. Using the *fitexy* procedure we obtained a slope of $\mu = 0.58 \pm 0.13$. A positive correlation is at odds with what would be expected if EW and Γ were strongly related. However, the sample we used includes both type-I and type-II AGN; considering only type-I objects, consistently to what is usually done for the X-ray Baldwin effect, the correlation is not significant anymore ($P_n = 54\%$).

5 DISCUSSION

In the last years several works have found a clear correlation between the X-ray photon index and the Eddington ratio (e.g., Shemmer et al. 2008, Fanali et al. 2013). Discordant results have been obtained when looking for a correlation between the X-ray luminosity and the photon index. While some works found an anti-correlation (e.g., Green et al. 2009; Young et al. 2009; Corral et al. 2011), others found a positive correlation (e.g., Dai et al. 2004; Saez et al. 2008), and many did not find any trend between the two parameters (e.g., Nandra & Pounds 1994; George et al. 2000; Reeves & Turner 2000; Page et al. 2005; Vignali et al. 2005; Shemmer et al. 2005, 2006; Just et al. 2007; Risaliti et al. 2009). For individual AGN several works found a tight correlation between Γ and L_{2-10} (e.g., Magdziarz et al. 1998; Zdziarski et al. 2003; Sobolewska & Papadakis 2009), which also points towards λ_{Edd} being the main driver of the observed trend. Changes in luminosity for individual objects are in fact directly related to changes

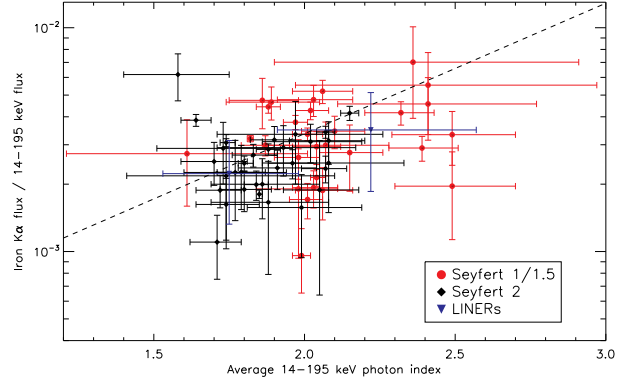


Figure 7. Ratio between the iron $K\alpha$ line flux measured by *Suzaku* (Fukazawa et al. 2011) and the 14–195 keV *Swift*/BAT flux (Baumgartner et al. 2010) versus the *Swift*/BAT photon index. The dashed line represents the linear fit to the data obtained using the *fitexy* procedure.

of the Eddington ratio. In this work we have studied the influence of the $\Gamma - \lambda_{\text{Edd}}$ relation on the $EW - \lambda_{\text{Edd}}$ trend for different geometries of the reflecting material. We have found that assuming $\Gamma \propto 0.31 \log \lambda_{\text{Edd}}$ as found by Shemmer et al. (2008) it is not possible to completely reproduce the observed $EW - \lambda_{\text{Edd}}$ correlation, with the average slope produced being at most $B \simeq -0.08$ for the toroidal geometry, $B \simeq -0.04$ for the spherical toroidal geometry and $B \simeq -0.05$ for the slab geometry.

Recently the $\Gamma - \lambda_{\text{Edd}}$ correlation has been confirmed by the study of Risaliti et al. (2009) on a large sample of ~ 400 Sloan Digital Sky Survey quasars with available *XMM-Newton* X-ray spectra. In their work Risaliti et al. (2009) found a trend consistent with that observed by Shemmer et al. (2008) when studying objects with black hole masses estimates obtained using $H\beta$, Mg II and C IV. When considering only the ~ 80 objects with values of M_{BH} obtained with $H\beta$ the correlation becomes stronger ($\Gamma \propto 0.58 \log \lambda_{\text{Edd}}$), while it is weaker or absent using only objects with Mg II and C IV measurements, respectively. The existence of differences between these trends has been interpreted by Risaliti et al. (2009) as being due to the different uncertainties on M_{BH} obtained from the three lines. While C IV is believed to be a poor estimator of the mass of the supermassive black hole (e.g., Netzer et al. 2007), both $H\beta$ and Mg II are thought to be produced in virialised gas and thus expected to be good mass indicators. However Mg II is a doublet and can be affected by contamination of Fe II, so that $H\beta$ is likely to be the best mass indicator. If, as argued by Risaliti et al. (2009), the $\Gamma - \lambda_{\text{Edd}}$ trend obtained using black-hole mass estimates from $H\beta$ is the most reliable, then the influence on the X-ray Baldwin effect should be more important. A result consistent with that of Risaliti et al. (2009) has been obtained by Jin et al. (2012) using black-hole mass estimates obtained from $H\alpha$ and $H\beta$, while Brightman et al. (2013) using $H\alpha$ and Mg II found a flatter slope (0.32 ± 0.05). Performing the same simulations of Sect. 3.1–3.3 using the $\Gamma - \lambda_{\text{Edd}}$ correlation found by Risaliti et al. (2009) using $H\beta$, we obtained values of B between -0.093 (for $\log N_{\text{H}}^{\text{T}} = 22.5$) and -0.14 (for $\log N_{\text{H}}^{\text{T}} = 25$) for the toroidal geometry, between -0.008 (for $\theta_{\text{OA}} = 70^\circ$ and $\log N_{\text{H}}^{\text{T}} = 22.6$) and -0.07 (for $\theta_{\text{OA}} = 10^\circ$ and $\log N_{\text{H}}^{\text{T}} = 24.5$) for the spherical-toroidal geometry, and of -0.11 (for $R = 1$) for the slab geometry. Repeating the Monte-Carlo simulations of Sect. 3.5 adopting the λ_{Edd} distribu-

³ In Fukazawa et al. (2011) a total of 88 AGN are reported, but NGC 1142 and Swift J0255.2–0011 are the same source.

tion of Vasudevan et al. (2010) and using the results of Risaliti et al. (2009) we found an average value of $B \simeq -0.147$ ($\sigma = 0.009$) for the toroidal geometry, $B \simeq -0.09$ ($\sigma = 0.04$) for the spherical-toroidal geometry, and of $B \simeq -0.09$ ($\sigma = 0.03$) for the slab geometry. Thus for all the geometries, assuming this steeper $\Gamma - \lambda_{\text{Edd}}$ relation one obtains slopes consistent within 1σ with the time-averaged (i.e. fits per source) $EW - \lambda_{\text{Edd}}$ trend.

Gu & Cao (2009), studying a sample of low luminosity AGN (LLAGN), which included low-ionisation nuclear emission line regions (LINERs) and local Seyfert galaxies with $\log \lambda_{\text{Edd}} \lesssim -2$, found that, contrarily to what has been observed at higher values of Eddington ratios, for these objects the photon index appears to be anti-correlated to λ_{Edd} . They found that $\Gamma \propto (-0.09 \pm 0.03) \log \lambda_{\text{Edd}}$, and argued that, as the anti-correlation is consistent with that found for X-ray binaries (XRB) in a low/hard state (e.g., Yamaoka et al. 2005), LLAGN and XRB in low/hard state might have a similar accretion mechanism, possibly an advection-dominated accretion flow (ADAF; see also Qiao & Liu 2012). A stronger anti-correlation has been found by Younes et al. (2011) studying a sample of 13 LINERs ($\Gamma \propto -0.31 \log \lambda_{\text{Edd}}$). These results might be used to constrain the importance of the $\Gamma - \lambda_{\text{Edd}}$ correlation on the X-ray Baldwin effect. The detection of a significant flattening or of a positive correlation between EW and λ_{Edd} for $\log \lambda_{\text{Edd}} \lesssim -2$ would in fact point towards an important impact on the observed $EW - \lambda_{\text{Edd}}$ relation.

In order to understand which is the mechanism responsible for the X-ray Baldwin effect it is fundamental to assess whether its main driver is the luminosity or rather the Eddington ratio. Our analysis of the *Chandra*/HEG sample of Shu et al. (2010) seems to indicate that the correlation of EW with the X-ray luminosity is stronger than that with the Eddington ratio. This would point towards a marginal role of the $\Gamma - \lambda_{\text{Edd}}$ trend on the decline of the iron $K\alpha$ EW with the luminosity and the Eddington ratio, although the significant uncertainties associated to κ_{X} and M_{BH} do not allow us to reach a firm conclusion. A possible alternative explanation for the X-ray Baldwin effect is that it is related to the decrease of the covering factor of the torus with the luminosity. Such a trend has been observed in a large number of studies performed at different wavelengths (e.g., Ueda et al. 2003, Beckmann et al. 2009), and it is likely to be the cause of the different luminosity distributions of type-I and type-II AGN (e.g., Ricci et al. 2011). In a recent work (Ricci et al. 2013), simulating the X-ray spectra of type-I populations with luminosity-evolving tori, we have shown that such an effect is able to reproduce the slope of the X-ray Baldwin effect for a large range of values of equatorial column densities of the torus ($\log N_{\text{H}}^{\text{T}} \gtrsim 23.1$). In order to discern between these two explanations, it is necessary to understand whether the slope of the $\Gamma - \lambda_{\text{Edd}}$ relation is as steep as $\simeq -0.6$ (e.g., Risaliti et al. 2009) or rather flatter ($\simeq -0.3$), as shown by several works (e.g., Shemmer et al. 2008).

6 SUMMARY AND CONCLUSIONS

In this work we have studied the influence of the $\Gamma - \lambda_{\text{Edd}}$ relation on the observed $EW - \lambda_{\text{Edd}}$ trend, assuming three different geometries for the reprocessing material. Our main results are the following.

- Applying bolometric corrections we found that the $EW - \lambda_{\text{Edd}}$ trend has a slope of $B = -0.13 \pm 0.03$ (in the *per source* case), and that it appears to be less significant than the $EW - L_{2-10}$ relation.
- Using the $\Gamma - \lambda_{\text{Edd}}$ relation of Shemmer et al. (2008) it is not

possible to fully account for the X-ray Baldwin effect for none of the geometries considered here, the slopes produced being flatter than the observed one.

- The relation between EW and Γ is dominated by scatter, and no clear anti-correlation is observed.
- Using the *Chandra*/HEG sample we found a weaker dependence of the photon index on the Eddington ratio ($\Gamma \propto 0.12 \log \lambda_{\text{Edd}}$) than that obtained by Shemmer et al. (2008). This might be related to the additional scatter introduced by the different sampling we used for λ_{Edd} and Γ .
- If the recent results of Risaliti et al. (2009) and Jin et al. (2012), who found a steeper correlation between photon index and Eddington ratio than that of Shemmer et al. (2008), were to be confirmed, then the $\Gamma - \lambda_{\text{Edd}}$ correlation might be able to produce slopes consistent with the X-ray Baldwin effect.

Our findings show that a good knowledge of the slope of the $\Gamma - \lambda_{\text{Edd}}$ relation is critical to understand whether this trend plays a leading or rather a marginal role in the X-ray Baldwin effect. A relation as steep as that found by Risaliti et al. (2009) would point towards a leading role, while a flatter trend, as that obtained by Shemmer et al. (2008), would imply that the X-ray Baldwin effect is driven by another mechanism. A plausible candidate would be the decrease of the covering factor of the molecular torus with the luminosity, which, as recently shown in Ricci et al. (2013), can straightforwardly explain the observed decline of the iron $K\alpha$ EW with the luminosity.

APPENDIX A: $\Gamma - EW$ DATA

In Table A1 the values of the average photon index of the *Chandra*/HEG sample of Shu et al. (2010) are listed, together with their references.

ACKNOWLEDGEMENTS

We thank R. Sato for his help, Chin Shin Chang and Poshak Gandhi for their comments on the manuscript. CR thanks P.O. Petrucci, the Sherpa group and IPAG for hospitality during his stay in Grenoble. We thank the anonymous referee for his/her comments that helped improving the paper. CR is a Fellow of the Japan Society for the Promotion of Science (JSPS). This work was partly supported by the Grant-in-Aid for Scientific Research 23540265 (YU) from the Ministry of Education, Culture, Sports, Science and Technology of Japan (MEXT). This research has made use of the NASA/IPAC Extragalactic Database (NED) which is operated by the Jet Propulsion Laboratory, of the High Energy Astrophysics Science Archive Research Center (HEASARC), provided by NASA's Goddard Space Flight Center, and of the SIMBAD Astronomical Database which is operated by the Centre de Données astronomiques de Strasbourg.

REFERENCES

- Anders E., Ebihara M., 1982, *Geochim. Cosmochim. Acta*, 46, 2363
- Andrade-Velázquez M., Krongold Y., Elvis M., et al., 2010, *ApJ*, 711, 888
- Arnaud K. A., 1996, in *Astronomical Data Analysis Software and Systems V*, edited by G. H. Jacoby & J. Barnes, vol. 101 of *Astronomical Society of the Pacific Conference Series*, 17

Table A1. (1) Average values and (2) references of the photon index of the objects in the *Chandra*/HEG sample of Shu et al. (2010).

Source	(1) < Γ >	(2) References
Fairall 9	1.85 ± 0.04	Gondoin et al. (2001b); Emmanoulopoulos et al. (2011); Patrick et al. (2011); McKernan et al. (2007)
NGC 526a	1.46 ± 0.02	Guainazzi et al. (2011)
Mrk 590	1.65 ± 0.03	Gallo et al. (2006); Longinotti et al. (2007)
NGC 985	1.60 ± 0.02	Krongold et al. (2005, 2009)
ESO 198–G24	1.82 ± 0.02	Porquet et al. (2004a); Winter et al. (2012)
3C 120	1.72 ± 0.02	McKernan et al. (2007); Miyazawa et al. (2009); Brightman & Nandra (2011)
NGC 2110	1.67 ± 0.03	Evans et al. (2007); Miyazawa et al. (2009)
PG 0844+349	2.06 ± 0.02	Gallo et al. (2011)
Mrk 705	2.2 ± 0.2	Gallo et al. (2005)
MCG –5–23–16	1.79 ± 0.02	Dewangan et al. (2003); Braitto et al. (2007); Reeves et al. (2007); Guainazzi et al. (2011)
NGC 3227	1.56 ± 0.07	Gondoin et al. (2003); Markowitz et al. (2009)
NGC 3516	1.93 ± 0.02	Turner et al. (2005); Markowitz et al. (2008); Turner et al. (2011)
NGC 3783	1.71 ± 0.04	Kaspi et al. (2001); Blustin et al. (2002); Netzer et al. (2003); Reeves et al. (2004); Reis et al. (2012)
NGC 4051	1.97 ± 0.02	Ponti et al. (2006); Lobban et al. (2011)
NGC 4151	1.96 ± 0.04	Cappi et al. (2006); Lubiński et al. (2010); Wang et al. (2010)
Mrk 766	2.23 ± 0.04	Boller et al. (2001); Turner et al. (2007); Risaliti et al. (2011)
3C 273	1.71 ± 0.07	Soldi et al. (2008)
NGC 4593	1.76 ± 0.02	Steenbrugge et al. (2003); Brenneman et al. (2007); McKernan et al. (2007); Markowitz & Reeves (2009)
MCG –6–30–15	1.94 ± 0.01	Wilms et al. (2001); Lee et al. (2002); Fabian et al. (2002); Chiang & Fabian (2011)
IRAS 13349+2438	2.07 ± 0.09	Longinotti et al. (2003); Holczer et al. (2007)
IC 4329A	1.81 ± 0.02	Gondoin et al. (2001a); McKernan & Yaqoob (2004); Steenbrugge et al. (2005); Miyazawa et al. (2009)
Mrk 279	1.66 ± 0.02	McKernan et al. (2007); Costantini et al. (2010)
NGC 5506	1.90 ± 0.02	Bianchi et al. (2003); Miyazawa et al. (2009); Guainazzi et al. (2010)
NGC 5548	1.61 ± 0.02	Andrade-Velázquez et al. (2010); de La Calle Pérez et al. (2010); Liu et al. (2010)
Mrk 290	1.66 ± 0.01	Zhang et al. (2011)
PDS 456	2.26 ± 0.02	Reeves et al. (2003, 2009); Behar et al. (2010)
E1821+643	1.84 ± 0.05	Fang et al. (2002); Jiménez-Bailón et al. (2007); Russell et al. (2010)
3C 382	1.77 ± 0.02	Gliozzi et al. (2007); Sambruna et al. (2011)
IRAS 18325–5926	2.01 ± 0.09	Mocz et al. (2011)
4C +74.26	1.85 ± 0.02	Ballantyne & Fabian (2005); Larsson et al. (2008)
Mrk 509	1.73 ± 0.01	Yaqoob et al. (2003b); Ponti et al. (2009); Noda et al. (2011); Petrucci et al. (2013)
NGC 7213	1.72 ± 0.01	Starling et al. (2005); Bianchi et al. (2008); Lobban et al. (2010)
NGC 7314	1.90 ± 0.02	Yaqoob et al. (2003a); Ebrero et al. (2011)
Ark 564	2.48 ± 0.02	Matsumoto et al. (2004); Vignali et al. (2004); Miyazawa et al. (2009); Singh et al. (2011)
MR 2251–178	1.55 ± 0.02	Gibson et al. (2005); Ramírez et al. (2008)
NGC 7469	1.79 ± 0.01	Blustin et al. (2003); Scott et al. (2005); Blustin et al. (2007); Patrick et al. (2011)

Baldwin J. A., 1977, *ApJ*, 214, 679Ballantyne D. R., Fabian A. C., 2005, *ApJ*, 622, L97Baumgartner W. H., Tueller J., Markwardt C., Skinner G., 2010, in *AAS/High Energy Astrophysics Division #11*, vol. 42 of *Bulletin of the American Astronomical Society*, 675Beckmann V., Soldi S., Ricci C., et al., 2009, *A&A*, 505, 417Behar E., Kaspi S., Reeves J., Turner T. J., Mushotzky R., O'Brien P. T., 2010, *ApJ*, 712, 26Bian W.-H., 2005, *Chinese Journal of Astronomy and Astrophysics Supplement*, 5, 289Bianchi S., Balestra I., Matt G., Guainazzi M., Perola G. C., 2003, *A&A*, 402, 141Bianchi S., Guainazzi M., Matt G., Fonseca Bonilla N., 2007, *A&A*, 467, L19Bianchi S., La Franca F., Matt G., et al., 2008, *MNRAS*, 389, L52Blustin A. J., Branduardi-Raymont G., Behar E., et al., 2002, *A&A*, 392, 453Blustin A. J., Branduardi-Raymont G., Behar E., et al., 2003, *A&A*, 403, 481Blustin A. J., Kriss G. A., Holczer T., et al., 2007, *A&A*, 466, 107

- Boller T., Brandt W. N., Fink H., 1996, *A&A*, 305, 53
- Boller T., Keil R., Trümper J., O'Brien P. T., Reeves J., Page M., 2001, *A&A*, 365, L146
- Braito V., Reeves J. N., Dewangan G. C., et al., 2007, *ApJ*, 670, 978
- Brandt N., Boller T., 1998, *Astronomische Nachrichten*, 319, 7
- Brandt W. N., Mathur S., Elvis M., 1997, *MNRAS*, 285, L25
- Brenneman L. W., Reynolds C. S., Wilms J., Kaiser M. E., 2007, *ApJ*, 666, 817
- Brightman M., Nandra K., 2011, *MNRAS*, 413, 1206
- Brightman M., Silverman J. D., Mainieri V., et al., 2013, *MNRAS*
- Cappi M., Panessa F., Bassani L., et al., 2006, *A&A*, 446, 459
- Chiang C.-Y., Fabian A. C., 2011, *MNRAS*, 414, 2345
- Corral A., Della Ceca R., Caccianiga A., et al., 2011, *A&A*, 530, A42
- Costantini E., Kaastra J. S., Korista K., et al., 2010, *A&A*, 512, A25
- Dai X., Chartas G., Eracleous M., Garmire G. P., 2004, *ApJ*, 605, 45
- de La Calle Pérez I., Longinotti A. L., Guainazzi M., et al., 2010, *A&A*, 524, A50
- De Marco B., Ponti G., Cappi M., et al., 2013, *MNRAS*, 431, 2441
- Denney K. D., Peterson B. M., Pogge R. W., et al., 2010, *ApJ*, 721, 715
- Dewangan G. C., Griffiths R. E., Schurch N. J., 2003, *ApJ*, 592, 52
- Ebrero J., Costantini E., Kaastra J. S., de Marco B., Dadina M., 2011, *A&A*, 535, A62
- Emmanoulopoulos D., Papadakis I. E., McHardy I. M., Nicastro F., Bianchi S., Arévalo P., 2011, *MNRAS*, 415, 1895
- Evans D. A., Lee J. C., Turner T. J., Weaver K. A., Marshall H. L., 2007, *ApJ*, 671, 1345
- Fabian A. C., Vaughan S., Nandra K., et al., 2002, *MNRAS*, 335, L1
- Fanali R., Caccianiga A., Severgnini P., et al., 2013, *MNRAS*, 433, 648
- Fang T., Davis D. S., Lee J. C., Marshall H. L., Bryan G. L., Canizares C. R., 2002, *ApJ*, 565, 86
- Fukazawa Y., Hiragi K., Mizuno M., et al., 2011, *ApJ*, 727, 19
- Gallo L. C., Balestra I., Costantini E., et al., 2005, *A&A*, 442, 909
- Gallo L. C., Grupe D., Schartel N., et al., 2011, *MNRAS*, 412, 161
- Gallo L. C., Lehmann I., Pietsch W., et al., 2006, *MNRAS*, 365, 688
- George I. M., Fabian A. C., 1991, *MNRAS*, 249, 352
- George I. M., Turner T. J., Yaqoob T., et al., 2000, *ApJ*, 531, 52
- Gibson R. R., Marshall H. L., Canizares C. R., Lee J. C., 2005, *ApJ*, 627, 83
- Gliozzi M., Sambruna R. M., Eracleous M., Yaqoob T., 2007, *ApJ*, 664, 88
- Gondoin P., Barr P., Lumb D., Oosterbroek T., Orr A., Parmar A. N., 2001a, *A&A*, 378, 806
- Gondoin P., Lumb D., Siddiqui H., Guainazzi M., Schartel N., 2001b, *A&A*, 373, 805
- Gondoin P., Orr A., Lumb D., Siddiqui H., 2003, *A&A*, 397, 883
- Green P. J., Aldcroft T. L., Richards G. T., et al., 2009, *ApJ*, 690, 644
- Grupe D., 2004, *AJ*, 127, 1799
- Grupe D., Komossa S., Leighly K. M., Page K. L., 2010, *ApJS*, 187, 64
- Gu M., Cao X., 2009, *MNRAS*, 399, 349
- Guainazzi M., Bianchi S., de La Calle Pérez I., Dovčiak M., Longinotti A. L., 2011, *A&A*, 531, A131
- Guainazzi M., Bianchi S., Matt G., et al., 2010, *MNRAS*, 406, 2013
- Holczer T., Behar E., Kaspi S., 2007, *ApJ*, 663, 799
- Ikeda S., Awaki H., Terashima Y., 2009, *ApJ*, 692, 608
- Iwasawa K., Taniguchi Y., 1993, *ApJ*, 413, L15
- Jiang P., Wang J. X., Wang T. G., 2006, *ApJ*, 644, 725
- Jiménez-Bailón E., Santos-Lleó M., Piconcelli E., Matt G., Guainazzi M., Rodríguez-Pascual P., 2007, *A&A*, 461, 917
- Jin C., Ward M., Done C., 2012, *MNRAS*, 425, 907
- Just D. W., Brandt W. N., Shemmer O., et al., 2007, *ApJ*, 665, 1004
- Kaspi S., Brandt W. N., Netzer H., et al., 2001, *ApJ*, 554, 216
- Kelly B. C., Bechtold J., Siemiginowska A., Aldcroft T., Sobolewska M., 2007, *ApJ*, 657, 116
- Korista K., Baldwin J., Ferland G., 1998, *ApJ*, 507, 24
- Krongold Y., Jiménez-Bailón E., Santos-Lleo M., et al., 2009, *ApJ*, 690, 773
- Krongold Y., Nicastro F., Elvis M., Brickhouse N. S., Mathur S., Zezas A., 2005, *ApJ*, 620, 165
- Larsson J., Fabian A. C., Ballantyne D. R., Miniutti G., 2008, *MNRAS*, 388, 1037
- Lee J. C., Iwasawa K., Houck J. C., Fabian A. C., Marshall H. L., Canizares C. R., 2002, *ApJ*, 570, L47
- Liu Y., Elvis M., McHardy I. M., et al., 2010, *ApJ*, 710, 1228
- Lobban A. P., Reeves J. N., Miller L., et al., 2011, *MNRAS*, 414, 1965
- Lobban A. P., Reeves J. N., Porquet D., et al., 2010, *MNRAS*, 408, 551
- Longinotti A. L., Bianchi S., Santos-Lleo M., et al., 2007, *A&A*, 470, 73
- Longinotti A. L., Cappi M., Nandra K., Dadina M., Pellegrini S., 2003, *A&A*, 410, 471
- Lubiński P., Zdziarski A. A., 2001, *MNRAS*, 323, L37
- Lubiński P., Zdziarski A. A., Walter R., et al., 2010, *MNRAS*, 408, 1851
- Magdziarz P., Blaes O. M., Zdziarski A. A., Johnson W. N., Smith D. A., 1998, *MNRAS*, 301, 179
- Magdziarz P., Zdziarski A. A., 1995, *MNRAS*, 273, 837
- Marchese E., Della Ceca R., Caccianiga A., Severgnini P., Corral A., Fanali R., 2012, *A&A*, 539, A48
- Marconi A., Risaliti G., Gilli R., Hunt L. K., Maiolino R., Salvati M., 2004, *MNRAS*, 351, 169
- Markowitz A., Reeves J. N., George I. M., et al., 2009, *ApJ*, 691, 922
- Markowitz A., Reeves J. N., Miniutti G., et al., 2008, *PASJ*, 60, 277
- Markowitz A. G., Reeves J. N., 2009, *ApJ*, 705, 496
- Matsumoto C., Leighly K. M., Marshall H. L., 2004, *ApJ*, 603, 456
- Mattson B. J., Weaver K. A., Reynolds C. S., 2007, *ApJ*, 664, 101
- McKernan B., Yaqoob T., 2004, *ApJ*, 608, 157
- McKernan B., Yaqoob T., Reynolds C. S., 2007, *MNRAS*, 379, 1359
- Middleton M., Done C., Schurch N., 2008, *MNRAS*, 383, 1501
- Miyazawa T., Haba Y., Kunieda H., 2009, *PASJ*, 61, 1331
- Mocz P., Lee J. C., Iwasawa K., Canizares C. R., 2011, *ApJ*, 729, 30
- Murphy K. D., Yaqoob T., 2009, *MNRAS*, 397, 1549
- Nandra K., 2006, *MNRAS*, 368, L62

- Nandra K., George I. M., Mushotzky R. F., Turner T. J., Yaqoob T., 1997, *ApJ*, 488, L91
- Nandra K., Pounds K. A., 1994, *MNRAS*, 268, 405
- Nayakshin S., 2000, *ApJ*, 534, 718
- Netzer H., Kaspi S., Behar E., et al., 2003, *ApJ*, 599, 933
- Netzer H., Lira P., Trakhtenbrot B., Shemmer O., Cury I., 2007, *ApJ*, 671, 1256
- Noda H., Makishima K., Yamada S., Torii S., Sakurai S., Nakazawa K., 2011, *PASJ*, 63, 925
- Page K. L., O'Brien P. T., Reeves J. N., Turner M. J. L., 2004, *MNRAS*, 347, 316
- Page K. L., Reeves J. N., O'Brien P. T., Turner M. J. L., 2005, *MNRAS*, 364, 195
- Patrick A. R., Reeves J. N., Porquet D., Markowitz A. G., Lobban A. P., Terashima Y., 2011, *MNRAS*, 411, 2353
- Perola G. C., Matt G., Cappi M., et al., 2002, *A&A*, 389, 802
- Peterson B. M., Ferrarese L., Gilbert K. M., et al., 2004, *ApJ*, 613, 682
- Petrucchi P. O., Henri G., Maraschi L., et al., 2002, *A&A*, 388, L5
- Petrucchi P.-O., Paltani S., Malzac J., et al., 2013, *A&A*, 549, A73
- Ponti G., Cappi M., Vignali C., et al., 2009, *MNRAS*, 394, 1487
- Ponti G., Miniutti G., Cappi M., Maraschi L., Fabian A. C., Iwasawa K., 2006, *MNRAS*, 368, 903
- Porquet D., Kaastra J. S., Page K. L., O'Brien P. T., Ward M. J., Dubau J., 2004a, *A&A*, 413, 913
- Porquet D., Reeves J. N., O'Brien P., Brinkmann W., 2004b, *A&A*, 422, 85
- Press W. H., Teukolsky S. A., Vetterling W. T., Flannery B. P., 1992, *Numerical recipes in FORTRAN. The art of scientific computing*
- Qiao E., Liu B. F., 2012, *ApJ*, 744, 145
- Ramírez J. M., Komossa S., Burwitz V., Mathur S., 2008, *ApJ*, 681, 965
- Reeves J. N., Awaki H., Dewangan G. C., et al., 2007, *PASJ*, 59, 301
- Reeves J. N., Nandra K., George I. M., Pounds K. A., Turner T. J., Yaqoob T., 2004, *ApJ*, 602, 648
- Reeves J. N., O'Brien P. T., Braitto V., et al., 2009, *ApJ*, 701, 493
- Reeves J. N., O'Brien P. T., Ward M. J., 2003, *ApJ*, 593, L65
- Reeves J. N., Turner M. J. L., 2000, *MNRAS*, 316, 234
- Reis R. C., Fabian A. C., Reynolds C. S., et al., 2012, *ApJ*, 745, 93
- Remillard R. A., McClintock J. E., 2006, *ARA&A*, 44, 49
- Ricci C., Paltani S., Awaki H., Petrucci P.-O., Ueda Y., Brightman M., 2013, *A&A*, 553, A29
- Ricci C., Walter R., Courvoisier T. J.-L., Paltani S., 2011, *A&A*, 532, A102
- Risaliti G., Nardini E., Salvati M., et al., 2011, *MNRAS*, 410, 1027
- Risaliti G., Young M., Elvis M., 2009, *ApJ*, 700, L6
- Russell H. R., Fabian A. C., Sanders J. S., et al., 2010, *MNRAS*, 402, 1561
- Saez C., Chartas G., Brandt W. N., et al., 2008, *AJ*, 135, 1505
- Sambruna R. M., Tombesi F., Reeves J. N., et al., 2011, *ApJ*, 734, 105
- Schulze A., Wisotzky L., 2010, *A&A*, 516, A87
- Scott J. E., Kriss G. A., Lee J. C., et al., 2005, *ApJ*, 634, 193
- Shemmer O., Brandt W. N., Netzer H., Maiolino R., Kaspi S., 2006, *ApJ*, 646, L29
- Shemmer O., Brandt W. N., Netzer H., Maiolino R., Kaspi S., 2008, *ApJ*, 682, 81
- Shemmer O., Brandt W. N., Vignali C., et al., 2005, *ApJ*, 630, 729
- Shields J. C., 2007, in *The Central Engine of Active Galactic Nuclei*, edited by L. C. Ho, J.-W. Wang, vol. 373 of *Astronomical Society of the Pacific Conference Series*, 355
- Shu X. W., Wang J. X., Yaqoob T., Jiang P., Zhou Y. Y., 2012, *ApJ*, 744, L21
- Shu X. W., Yaqoob T., Wang J. X., 2010, *ApJS*, 187, 581
- Silva L., Maiolino R., Granato G. L., 2004, *MNRAS*, 355, 973
- Singh V., Shastri P., Risaliti G., 2011, *A&A*, 532, A84
- Sobolewska M. A., Papadakis I. E., 2009, *MNRAS*, 399, 1597
- Soldi S., Türler M., Paltani S., et al., 2008, *A&A*, 486, 411
- Starling R. L. C., Page M. J., Branduardi-Raymont G., Breeveld A. A., Soria R., Wu K., 2005, *MNRAS*, 356, 727
- Steenbrugge K. C., Kaastra J. S., Blustin A. J., et al., 2003, *A&A*, 408, 921
- Steenbrugge K. C., Kaastra J. S., Sako M., et al., 2005, *A&A*, 432, 453
- Turner T. J., Kraemer S. B., George I. M., Reeves J. N., Bottorff M. C., 2005, *ApJ*, 618, 155
- Turner T. J., Miller L., Kraemer S. B., Reeves J. N., 2011, *ApJ*, 733, 48
- Turner T. J., Miller L., Reeves J. N., Kraemer S. B., 2007, *A&A*, 475, 121
- Ueda Y., Akiyama M., Ohta K., Miyaji T., 2003, *ApJ*, 598, 886
- Vasudevan R. V., Fabian A. C., 2007, *MNRAS*, 381, 1235
- Vasudevan R. V., Fabian A. C., 2009, *MNRAS*, 392, 1124
- Vasudevan R. V., Fabian A. C., Gandhi P., Winter L. M., Mushotzky R. F., 2010, *MNRAS*, 402, 1081
- Vasudevan R. V., Mushotzky R. F., Winter L. M., Fabian A. C., 2009, *MNRAS*, 399, 1553
- Vestergaard M., 2002, *ApJ*, 571, 733
- Vignali C., Brandt W. N., Boller T., Fabian A. C., Vaughan S., 2004, *MNRAS*, 347, 854
- Vignali C., Brandt W. N., Schneider D. P., Kaspi S., 2005, *AJ*, 129, 2519
- Wang J., Mao Y. F., Wei J. Y., 2009, *AJ*, 137, 3388
- Wang J., Risaliti G., Fabbiano G., Elvis M., Zezas A., Karovska M., 2010, *ApJ*, 714, 1497
- Wang J.-M., Watarai K.-Y., Mineshige S., 2004, *ApJ*, 607, L107
- Wilms J., Reynolds C. S., Begelman M. C., et al., 2001, *MNRAS*, 328, L27
- Winter L. M., Mushotzky R. F., Reynolds C. S., Tueller J., 2009, *ApJ*, 690, 1322
- Winter L. M., Veilleux S., McKernan B., Kallman T. R., 2012, *ApJ*, 745, 107
- Woo J.-H., Urry C. M., 2002, *ApJ*, 579, 530
- Yamaoka K., Uzawa M., Arai M., Yamazaki T., Yoshida A., 2005, *Chinese Journal of Astronomy and Astrophysics Supplement*, 5, 273
- Yaqoob T., George I. M., Kallman T. R., Padmanabhan U., Weaver K. A., Turner T. J., 2003a, *ApJ*, 596, 85
- Yaqoob T., McKernan B., Kraemer S. B., et al., 2003b, *ApJ*, 582, 105
- Younes G., Porquet D., Sabra B., Reeves J. N., 2011, *A&A*, 530, A149
- Young M., Elvis M., Risaliti G., 2009, *ApJS*, 183, 17
- Zdziarski A. A., Lubiński P., Gilfanov M., Revnivtsev M., 2003, *MNRAS*, 342, 355
- Zhang S. N., Ji L., Marshall H. L., Longinotti A. L., Evans D., Gu Q. S., 2011, *MNRAS*, 410, 2274